2021

Photoemission Investigation of Topological Quantum Materials

Klauss M. Dimitri
University of Central Florida

PHOTOEMISSION INVESTIGATION OF TOPOLOGICAL QUANTUM MATERIALS

by

KLAUSS M. DIMITRI

A thesis submitted in partial fulfilment of the requirements
for the Honors in the Major Program in Physics
in the College of Science
and in the Burnett Honors College
at the University of Central Florida

Summer Term
2021

Thesis Chair: Madhab Neupane

ABSTRACT

Topological insulators (TIs) are a class of quantum materials, which behave as insulators in the bulk, yet possess gapless spin-polarized surface states, which are robust against nonmagnetic impurities. The unique properties of TIs make them attractive not only for studying various fundamental phenomena in condensed matter and particle physics, but also as promising candidates for applications ranging from spintronics to quantum computation. Within the topological insulator realm, a great deal of focus has been placed on discovering new quantum materials, however, ideal multi-modal quantum materials have yet to be found. Here we study α-$PdBi_2$, KFe_2Te_2, and DySb compounds including others within these families with high-resolution angle-resolved photoemission spectroscopy (ARPES) complimented by first principles calculations. We observe unique phase changes and phenomena across their transition temperatures. Our work paves a new direction in material discovery and application related to their unique electronic properties.

TABLE OF CONTENTS

LIST OF FIGURES vi

CHAPTER 1: INTRODUCTION 1

CHAPTER 2: LITERATURE REVIEW 4

Photoelectic effect 4

ARPES 4

Topological Insulators 5

Fermions 6

Quasi-particles 7

Dirac 7

Majorana 8

CHAPTER 3: METHODOLOGY 10

Crystal Growth and DFT 10

ARPES 10

Detailed, high quality, electronic structure study of DySb, α-$PdBi_2$, and KFe_2Te_2 . 12

Photon energy dependent measurements 12

Temperature dependent measurements 13

CHAPTER 4: RESULTS 14

DySb 14

Introduction 14

Results 15

Conclusion 20

α-$PdBi_2$ 21

Introduction 22

Results 24

Conclusion 29

Preliminary Results on KFe_2Te_2 29

CHAPTER 5: CONCLUSION 32

Future Work 32

Closing Remarks 33

LIST OF REFERENCES 34

LIST OF FIGURES

Figure 3.1: **Angle-resolved photo emission spectroscopy setup and process** 11

Figure 4.1: **Brillouin zone, electronic structure and sample characterization of DySb.** (a) Shows the rock salt-type cubic lattice crystal of DySb. (b) Schematic Brillouin zone and projected surface state of face centered DySb. (c) Spectroscopic measured core level spectrum of DySb, clearly observed sharp peak of Sb 4*d* and Dy 4*f*, 5*s* and 5*p*, which indicates the good quality of the samples. (d),(e) Bulk-band calculations along multiple high symmetry points of DySb without and with the consideration of spin orbit coupling, respectively. 16

Figure 4.2: **Measured Fermi surface and constant energy contours of DySb.** (a-e) ARPES measured Fermi surface mapping and constant energy contours with an incident photon energy of 60 eV and a temperature of around 16 K. The binding energies are noted in the plots. (f-g) constant energy contour calculations using SCAN. The binding energies are noted in the plots. All the experiments were performed at SIS-HRPES end-station at SLS, PSI at a temperature around 16 K. 17

Figure 4.3: **Observation of Dirac like state in DySb.** (a) ARPES measured dispersion along the X-Γ-X direction with an incident photon energy of 70 eV at a temperature of 6 K. (b) SCAN calculations for the X-Γ-X direction. (c) ARPES measured dispersion along the M-Γ-M direction with an incident photon energy of 70 eV at a temperature of 30 K. (d) SCAN calculations for the M-Γ-M direction. (e) ARPES measured dispersion along the X-M-X direction with an incident photon energy of 60 eV at a temperature of 30 K. (f) SCAN calculations for the X-M-X direction. All these measurements were performed at SIS-HRPES end-station at SLS, PSI all calculations were done considering the "f" electrons as core electrons. 19

Figure 4.4: **Photon energy dependent measurements of the Γ-X-Γ direction in DySb.** The High symmetry X point is measured at various photon energies from 55 eV to 70 eV in increments of 5 eV steps where a Dirac-like linearly dispersive state is observed in each plot. It is important to note that the rightmost image with 70eV photon energy was taken at ALS beamline 10.0.1 with a different sample at 17 K, the rest of the measurements were performed at SIS-HRPES end-station at SLS, PSI at a temperature around 16 K. 20

Figure 4.5: **α-$PdBi_2$ molecular structure and transport data** (a) Molecular structure of α-$PdBi_2$ where purple spheres are Bi atoms and blue spheres are Pd atoms (b) Momentum path in the $5 \times 1 \times 1$ supercell used for DFT calculations of α-$PdBi_2$. (c) Temperature dependent resistivity measurements. (d) Core level spectrum (e) $5 \times 1 \times 1$ supercell used for theoretical DFT calculations. 24

Figure 4.6: **Experimentally measured band structure of α-PdBi$_2$** (a) Electronic structure measurements cut along the A-Γ-A direction. (b) Fermi surface map of α-PdBi$_2$ (c) Binding energy measurments above, at and below the Dirac point 25

Figure 4.7: **Theory and Experimental comparison** (a) Dispersion map of α-PdBi$_2$ obtained at photon energies of 70, 76, and 84 eV 26

Figure 4.8: **Calculated band structures of α-PdBi$_2$** (a) Without SOC (b) With SOC (c) With SOC and a larger binding energy range extending over the Fermi level. 28

Figure 4.9: **Preliminary results for KFe$_2$Te$_2$.** (a) Molecular structure of KFe$_2$Te$_2$. (b) Band structure calculation for the Bicollinear anti-ferromagnetic order of KFe$_2$Te$_2$ with a magnetic moment of 2.6 μ_B (c) The integrated energy distribution curve for KFe$_2$Te$_2$. Inset shows a sample of KFe$_2$Te$_2$ where the sample is approximately 5 mm at its longest and 3 mm at its widest. 30

CHAPTER 1: INTRODUCTION

The discovery of Topological insulators (TIs)[1, 2] has motivated research in the direction of many different topological materials this includes topological nodal-line semimetals (TNLSs). These are materials that offer platforms for realizing many exotic physical phenomena and can be driven into various topological states including Dirac semimetals, Weyl semimetals, topological insulators, and quantum anomalous Hall insulators (QAHIs) by breaking certain symmetries (i.e. mirror symmetry) or including the spin orbit coupling (SOC) effect [1, 2]. TNLSs are unique such that in k-space the lowest conduction band and the highest valence band touch each other along 1D symmetry-protected lines, which can be found in several different forms. One of which, where the nodal-lines carry a quantized π-Berry phase and is protected by either crystalline symmetry or both inversion and time-reversal symmetry, is incredibly fascinating as it leads to a nearly flat drumhead-like state with an infinite density of states (DOS) on its boundary[1, 2]. These distinctly different properties provide TNLSs with some exotic characteristics including special long range Coulomb interactions, a unique Landau energy level, and even high temperature superconductivity [101]. This new investigative effort on TNLSs has recently begun to mesh itself with the everlasting quest of realizing high-temperature superconductivity. Since 2008, iron-based superconductors such as LaOFeAs [7], $BaFe_2As_2$ [8], α-FeSe(Te)[9], and $K_xFe_2 - ySe_2$ [10] have provided valuable insight into the interesting pairing mechanism of these materials and has given a direction for higher-superconducting temperatures. However, attempts at bridging the gap between these two phenomena, TNLSs and higher-temperature superconductive states, has been lacking. Such a connection between two distinct fields of condensed matter physics would not only establish a fascinating material and a new direction for further research but also develop significantly stronger communication and interest between the two areas of research.

Another direction that has been taken with topological insulators is that they can be exploited for

their high carrier mobility, extreme magnetoresistence (XMR), and their potential to revolutionize fields such as quantum computing, spintronics, and dozens more are reasons for their large current theoretical and experimental research interest [12, 14, 28, 51]. It is well known that the TIs can be characterized by their linearly dispersive gapless topological surface states (TSS) within the bulk insulating gap of inverted valence and conduction bands [12, 14, 28, 51]. Interest in these core characteristics invoked research that branched from the common TI to a great variety of gapless topological materials including the Dirac, Weyl, and nodal semimetals [52, 98, 54, 55, 56]. The Dirac fermionic states in these TIs and semimetals quickly became a sensation within the community as they provided a path for realizing novel exotic quantum states [1, 102]. Soon enough a link between the Dirac fermionic states and rare-earth monopnictides was made as they are predicted to host a 3D TI or topological Dirac semimetal at the X point of their bulk Brillouin zone [58] as well as impressive XMR values [59, 60, 61, 97, 63, 64, 65]. XMR materials have been recognized to be semimetals with nearly compensated electron and hole carriers. Interestingly, XMR has been reported in rare earth monopnictides such as LaSb, LaBi, and NdSb [69, 70, 71, 10, 73, 56]. In the last few years a rebirth of interest in these rare earth monopnictides has taken hold [69, 71, 74, 75, 76, 77, 78, 79, 80] as they are largely untapped systems for exploring XMR, topological semimetallic states, and especially f-electron correlations and their role in exotic phenomena.

Even though the rare earth monopnictides possess a simple NaCl-type structure, their diverse and unusual properties have garnered them plenty of attention. The condensed matter community's interest in these materials are a result of their potential applications as they have a complex interplay between magnetic moments, spin orbit coupling (SOC), and f-electron orbitals. In order to simulate and predict which monopnictide material systems would present themselves as interesting and useful to physics, it is important to have detailed explanation of the XMR in these systems. Currently, there are several mechanisms that propose an explanation of the XMR for monopnic-

tide systems including forbidden backscattering at zero field [69, 79], electron-hole compensation [71, 74, 76, 78, 80], and non-trivial band topology [74]. In addition to their perplexing XMR properties, a recent increase in interest regarding rare earth ions with f-electron systems, providing a tunable, strongly correlated magnetic ground states in the rare earth monopnictide family, has inspired others in the field to expand the database of materials that follow this direction. As a momentum-resolved probe of the electronic structure, capable of isolating the surface from the bulk states, angle resolved photoemission spectroscopy (ARPES) can systematically map the band structure of such materials and present convincing evidence for topological and spin-split surface states. For materials LaSb and CeSb, ARPES measurements have determined that there are no band inversions or crossings [74, 75, 77] suggesting they are topologically trivial. As such Dysprosium Antimonide (DySb) is currently a poorly studied antiferromagnetic (AFM) member of the rare earth monopnictide family and holds great promise to provide a promising direction in not only XMR but also in the role f-electron hybridization plays in these systems [81, 82, 83, 63]. Previous calculations on DySb predict a band inversion and therefore suggesting a topologically non-trivial state [63].

Therefore, here we utilize a high resolution angle-resolved photoemission spectroscopy (ARPES) setup to systematically study the normal, anti-ferromagnetic, and superconducting state electronic properties of KFe_2Te_2 as well as DySb and their respective families. We also plan to combine our ARPES technique with SCAN calculations within a DFT framework in order to best investigate a multi-modal system in KFe_2Te_2, as well as providing details of the gapped or non-gapped state in DySb. Our preliminary data and analysis on DySb potentially reveals the presence of trivial states with a small gap. We propose to provide a detailed study which has the potential to provide a deeper understanding of the 122 families of KFe_2Te_2 as well as the rare-earth monopnictide family of DySb.

CHAPTER 2: LITERATURE REVIEW

Photoelectic effect

One of the phenomena that is utilized most by the condensed matter field that is critical for accurately characterizing the electronic structure of any crystal system is the photoelectric effect. A phenomena that was first truly observed by Heinrich Hertz in 1887, and after that theoretically explained by Albert Einstein in 1905 for which he received the Nobel prize in physics. The process is when light with a high photon energy that exceeds a specific binding energy is incident upon the surface of a material, electrons are emitted [5]. These electrons are emitted at many different angles and with varying kinetic energies, as such they carry a significant amount of information about the system they are ejected from. These properties of the emitted electrons can be processed through an electron analyzer in order to determine the band structure of any one material.

ARPES

Angle-resolved photoemission spectroscopy (ARPES) is a strong technique that can analyze these emitted electrons in order to discern an accurate band structure. After using an electron analyzer to determine the energies in the occupied states, it builds a 3D representation of the electronic bandstructure of the analyzed material [98]. Physicists then dissect that 3D representation and from the patterns of electrons that are observed it is possible to determine unique and exciting phenomena that occurs within the system. During the last decade many different types of ARPES have been developed including spin-resolved ARPES, time-resolved ARPES, spatially resolved ARPES, and soft-X-ray ARPES. Although we will solely focus on traditional ARPES for this systematic experimental analysis.

Topological Insulators

A topological insulator (TI), as experimentally realized in bismuth-based materials, is a novel electronic state of quantum matter characterized by a bulk-insulating band gap and spin-polarized metallic surface states [1, 2]. Owing to time reversal symmetry, topological surface states are protected from backscattering and localization in the presence of weak perturbation, resulting in spin currents with reduced dissipation. This makes the discovery of TIs a revolutionary milestone in the field of materials physics. They hold major promise to be materials protected from electron backscattering at high temperatures, essentially providing the benefits of superconductors without the cost of cooling. A major characteristic of TIs are that they host strong spin-orbit coupling (SOC) and are a defining feature as it opens up a plethora of potential for developing new technologies and research directions [5, 6]. Bismuth-Antimony based materials were the first to experimentally realize the TI. Since SOC is a strong defining factor for TIs it is not surprising that the first TI was made from Bismuth (Bi) and Antimony (Sb). These two elements are heavy and contain many electrons and as such have a strong SOC, Bismuth just so happens to be the heaviest element that is not radioactive. Thus it may be clear as to why the first discovered TI would contain this element. Sb also has strong SOC, its electronic band structure has one band inversion which just so happens to be odd. As such this makes Sb topologically nontrivial where $\nu_0 = 0$. Unfortunately, Sb is a semimental, and as such does not contain a significant band gap in its electronic structure. By combining Sb with Bi certain energy levels can be tuned until a full band gap is achieved. From this we obtain the $Bi_{1-x}Sb_x$ alloys, the Bi_2X_3 (X = Se, Te) series, and their derivatives [1, 2]. The discovery of the TI tremendously accelerated research into phases of matter characterized by non-trivial topological invariants. Not only did the 3D Z_2 TI itself attract great research interest, it also inspired the prediction and experimental realization of a range of new topological phases of matter. Recently, the 3D Dirac semimetal phase has been experimentally realized in Cd_3As_2 and Na_3Bi [1, 2, 51], which have shown linear dispersion in all three-dimensions.

Similarly, the Weyl semimetal state in TaAs-class of material is established using photoemission spectroscopy, which identified the Fermi arc surface states and their unique odd number of Fermi surface crossings for a closed loop on the surface Brillouin zone and bulk Weyl cones [1, 2, 51]. The unique electronic structure of these topological Dirac and Weyl semimetals are not only alluring for their unusual electronic/magnetic properties, but also for providing a platform that can realize elementary particles such as the Dirac, Weyl, Nodal, and Majorana fermion phases.

Fermions

In order to continue on it is important to make a couple of notes about fermions such that it is possible to build certain concepts described in the rest of the document. To begin a fermion is a particle that obeys the Pauli exclusion principle and follow Fermi-Dirac statistics. This is different than bosons which do not obey the Pauli exclusion principle and instead follow Bose-Einstein statistics. All quarks, leptons, and baryons are defined as fermions as well as all atoms and nuclei made from an odd number of quarks and leptons. A Dirac fermion are relativistic fermions where E and P have a linear relationship, additionally it is not its own anti-particle, pretty much every particle on the standard model, except for neutrinos, fit this description. For example, electrons have positrons as their anti-particle whereas neutrinos have no charge and thus has a possibility of being its own anti-particle. On the other hand we have Majorana fermions, these are particles that are their own anti-particle, neutrinos may fit into this category but it is currently being debated within the particle physics community. In addition to this there are also Weyl fermions, which are a half of a Dirac fermion, Weyl fermions always come in pairs and they are of opposite chirality, when these two pairs come together they form a Dirac fermion.

Quasi-particles

Quasi-particles are an incredibly important aspect of this field, they are low binding energy excitations within a system that show similar characteristics to real particles. A good example of this is if a positron is traveling in a certain direction with a certain speed, the quasiparticle equivalent to this situation would be as if an electron were traveling with the same momentum but in the opposite direction. Quasiparticles as they are realized in Dirac, Majorana, and Weyl semimetals have a more complex nature to them . Each one of these semimetals has interesting properties that gives us reason to study and investigate them. Dirac and Weyl semimetals contain quasiparticles that allow the electrons within the system to behave relativistically and as such allows them to conduct electric charge much faster than typical electrons, this in turn could be used to create much faster electronic circuits [13]. Majorana semimetals contain Majorana quasiparticles, since they are their own anti-particles they can exist in a superpositions state, combined with the robustness given by topology, they form an ideal basic component for creating qubits that can power quantum computers.

Dirac

The Dirac semimetals are named after the relativistic fermions of solid state band structure and they trace back to 1947 when graphene was first discussed [4]. Graphene is known as a two dimensional semimetal with relativistic electrons, as such the symmetries innate to graphene protect its Dirac nature. Interest in two dimensional massless electrons in graphene allowed for the explosive interest in these same massless electrons to exist in other topological materials. The interest in 2D Dirac semimetals transistioned to an interest in 3D Dirac semimetals which has a high likelihood of being found in high SOC materials, the same kind that TIs are most likely to be found. A major reason for the interest in transitioning from 2D to 3D materials is that the Hamiltonian

adjusts itself from $H = v_F(p_x\sigma_x + p_y\sigma_y)$ to $H = v_F(p_x\sigma_x + p_y\sigma_y + p_z\sigma_z)$. Since in the latter case all three Pauli matrices are used, this means that there is no local mass term. This is theoretically very promising to find massless fermions which can then find its use in novel technologies. Essentially the unusually straight dispersion of bands that can be seen in the electronic structure of Dirac semimetals allows it to behave very relativisticly due to the massless properties that the electrons take within the system. This has enormous potential for building systems that run on low energy and fast speeds as the massless electrons can travel much faster. There are two major intrinsic Dirac semimetals, Na_3Bi and Cd_3As_2, most other Dirac semimetals are developed by tuning the bulk gap of other compounds. The quest for finding other Dirac semimetals is important as it allows us to expand our base of knowledge of these systems and their mechanisms, and since they are closely tied to other interesting systems such as TIs, it allows us to build a larger foundation of knowledge on these general topics.

Majorana

In direct opposition to the Dirac fermion, a Majorana fermion is its own antiparticle. It is not settled science but it is believed that the neutrino would be the only known particle to fit the category of Majorana fermion. Within the realm of condensed matter sciences, Majorana fermions typically appear in materials as quasiparticle excitations [100]. This is very common when dealing with superconductors because they have this unique property where a quasiparticle in a superconductor can exist as its own antiparticle. This is because from a theoretical standpoint, in a superconducting system the superconductor imposes an electron hole type of symmetry on quasiparticle excitations as it creates an annihilation operator the same time it creates a creation operator. These operators can exist at zero energy and are known as Majorana zero modes or Majorana bound states [13]. They are named such as they no longer follow fermionic statistics and can be categorized as non-abelian anyons [100]. The properties thes Majorana bound states now have make them ideal tools

to develop a topological quantum computer.

CHAPTER 3: METHODOLOGY

Crystal Growth and DFT

Details on the Sn flux technique utilized to grow the single crystal samples of DySb, α-$PdBi_2$, and KFe_2Te_2 can be found in other literature [84]. Our collaborators Dariusz Kaczorowski and Raman Sankar handle the crystal growing techniques for the three materials. For the systematic experimental measurements we plan to utilize syncrotron sources as well as our in lab setup. When measuring the ARPES system had an energy resolution better than 20 meV and an angular resolution better than 0.2°. The calculations for the electronic structure used a density functional theory (DFT) framework which also incorporated the projector augmented wave (PAW) method [85] as utilized in the VASP suite of codes [86, 87]. The exchange-correlation functional was treated using SCAN meta-GGA [88]. An energy cutoff of 400 eV was used for the plane-wave basis set and a Γ-centered $11\times11\times11$ k-mesh was used for BZ integrations. A tight-binding model with atom-centered Wannier functions using the VASP2WANNIER90 interface was created in order to investigate the topological properties of KFe_2Te_2 and DySb [89]. The iterative Green's function technique using the WannierTools package was used to obtain the surface energy spectrum [90, 91, 92].

ARPES

With almost five decades of both scientific and technical development, angle resolved photoemission spectroscopy (ARPES) is now one of the most prominent experimental techniques for exploring nearly all aspects of condensed-matter physics, from active frontiers such as low-dimensional semiconductors, high temperature superconductivity, topological phenomena, and solids that ex-

perience hybridization of electron orbitals to developing devices from novel spintronics to solar cells. ARPES measures the angle and momentum of electrons that are released from the solid due to radiation incident on the sample. The resulting momentum and energy relationship is a identical representation of the electronic structure of the sample, the raw data of ARPES is thus a direct presentation of the electronic structure of the sample being measured. In equilibrium, ARPES is capable of resolving occupied electronic state in momentum space. Today, a prototype ARPES system uses continuous incident radiation and a hemispherical electron analyzer to collect the photoelectrons as shown in Figure 3.1. Electrons with different kinetic energies and momenta are deflected and undergo different trajectories within the electron analyzer before they hit the phosphor screen and the CCD camera. The major advantage of the ARPES technique is that the light source needed for the process is readily available from many sources, since continuous ultraviolet to X-ray radiation is routinely produced by gas discharge lamps, continuous-wave lasers, and synchrotrons.

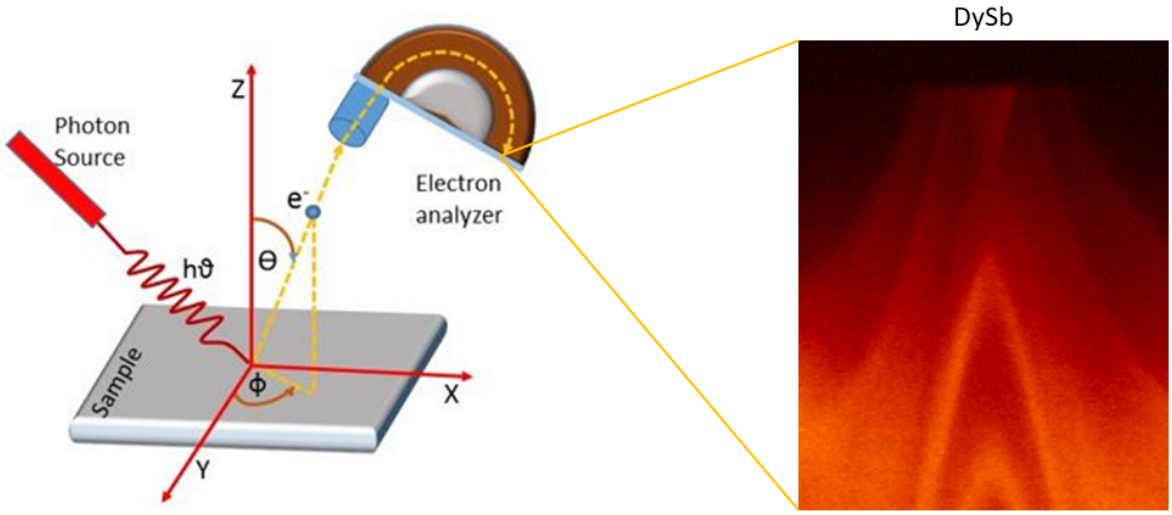

Figure 3.1: **Angle-resolved photo emission spectroscopy setup and process**

Since ARPES and its derivative techniques are the only known ways of isolating the bulk from

the surface states in topological materials, convincing evidence for the existence of these exciting emergent quantum phases can only be obtained with these spectroscopic tools. So far, photoemission spectroscopy combined with first-principles calculations has played a major role in the discovery of numerous topological phenomena and materials. Therefore, it is natural to propose the utilization of the spectroscopic probes for understanding and discovering novel phases of matter.

Detailed, high quality, electronic structure study of DySb, α-PdBi$_2$, and KFe$_2$Te$_2$

We will systematically analyze the electronic structure and band dispersion of DySb, α-PdBi$_2$, and KFe$_2$Te$_2$ as a function of the incident photon energy allowing us to measure the Fermi momentum and velocity of the k_x, k_y, and k_z momentum directions. Using the ARPES technique at low temperatures will allow us to obtain the detailed electronic structure of DySb, α-PdBi$_2$, and KFe$_2$Te$_2$ and create an accurate map of its Fermi surface. The overall experimental analysis will provide us with a detailed electronic structure and allow us to directly compare it with the first-principles calculations in order to reveal the true nature of DySb, α-PdBi$_2$, and KFe$_2$Te$_2$.

Photon energy dependent measurements

Once we have obtained our measurements of the Fermi surface and the rough band structure data of DySb, α-PdBi$_2$, and KFe$_2$Te$_2$ we will probe into the material to map the low-lying electronic structure with extreme care at various photon energies in order to gather enough conclusive evidence to establish the bulk and surface states within the electronic structure. By mapping the electronic structure at multiple photon energies we will be able to distinguish the surface states from the bulk states enabling us to conclude the nature of DySb, α-PdBi$_2$, and KFe$_2$Te$_2$ with more certainty.

Temperature dependent measurements

In order to reveal the robustness of the states we will repeat the previous experiments again at low temperatures after applying thermal recycling. The thermal recycling procedure shall begin when have our measurement equipment optimally focused on the phenomena of interest in KFe_2Te_2 at 10 K. From 10 K we incrementally increase the temperature by 5 K whilst taking measurements at each step until the desired temperature of 90 K is reached. The sample is then rapidly increased from 90 K to room temperature at 300 K and subsequently cooled to 10 K. Once again measurements are made and compared with the data obtained previous to the thermal recycling to determine the robustness of the states in KFe_2Te_2. As for DySb, as it has a Neel temperature of $T_N = 9K$ temperatures lower than this value will be obtained and recycled similar to the process with KFe_2Te_2.

CHAPTER 4: RESULTS

DySb

An incredible amount of interest has developed for the rare-earth monopnictide (REM) family as a direct result of its unique and unusual extreme magnetoresistance (XMR) properties and its potential to have non-trivial surface states. Here we study the the detailed electronic structure of DySb in an attempt to explain the origin of XMR in the rare-earth monopnictide family. By using both experimental and theoretical techniques including ARPES and DFT, we investigate the unique electronic states that exist in DySb.

Introduction

The unique and interesting properties found in topological insulators, which include high carrier mobility and XMR, have resulted in the immense interest that condensed matter researchers have developed for these classes of materials. Exploration of these systems have resulted in the discovery of many new and unique systems such as Dirac, Majorana, Weyl, and nodal-line systems that host a variety of unique phenomena [52, 98, 54, 55, 56]. Because of this, countless new directions have been developed that allow for the discovery of fascinating, novel phenomena that hold promise to allow for the development of new technologies such as spintronics and other low-power devices [102]. The rare-earth monopnictide family (REM) has been a subject of extreme interest as a family of materials that has enormous potential to realize 3D topological insulator states and topological Dirac semimetal materials [58]. Additionally, REM have proven to host XMR in multiple systems within its family [59, 60, 61]. The REM systems have also been speculated to be a promising system to tie topological states with XMR, which is a major current focus in the con-

densed matter community. Conventionally, the explanation for XMR has been the electron-hole compensation theory [60, 76, 103], but the prevalent presence of XMR within topological systems such as TaAs [104] as well as the REM family has stirred up the possibility that XMR may originate in the forbidden backscattering channels of topological systems [105]. Topological surface states have been observed in LaSb and LaBi [106, 107, 108, 109] and suggested in others such as LuBi and LaAs [59, 60, 61]. Additionally, a Dirac semimetal state has been suggested in other REM such as NdSb and HoSb [99]. As such with the foundation provided by these previous results it is important to conduct further theoretical and experimental research in order to obtain a deeper understanding of the connection between XMR and Dirac-like states.

REM materials are heavy and as such contain f-electron orbitals which means they have strong correlations and it is possible to tune their magnetic ground states. As we move along the rare earth elements there is an observed transition from nonmagnetic to ferromagnetic. We see that DySb is an antiferromagnetic REM member that lacks investigation [63]. Its strong XMR properties in addition to its antiferromagnetic nature provides a strong opportunity for us to investigate the origin of XMR in a Dirac-like semimetalic system, this would provide major insight into the nature of XMR within the REM systems.

Results

As for DySb, similar to other rare earth monopnictides, it adopts a NaCl-type crystal structure with space group $Fm-3m$ (225)(see Figure 1(a)). However, when transitioning into its antiferromagnetic state its crystal structure morphs into a tetragonal one by shrinking along the c axis at its Neel temperature T_N = 9 K (c/a = 0.993) [93], this shifts the space group into I4/mmm (139) [94].

Figure 2(b) depicts the surface and bulk Brillouin zone (BZ) of DySb. The high-symmetry points

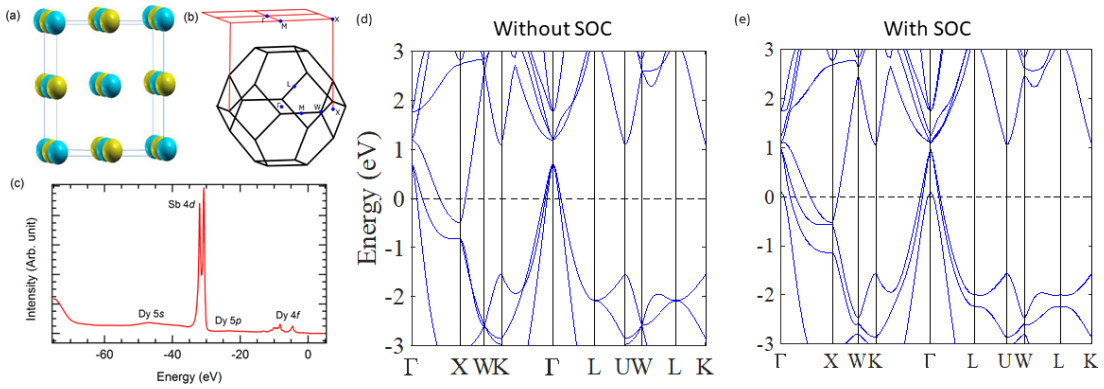

Figure 4.1: **Brillouin zone, electronic structure and sample characterization of DySb.** (a) Shows the rock salt-type cubic lattice crystal of DySb. (b) Schematic Brillouin zone and projected surface state of face centered DySb. (c) Spectroscopic measured core level spectrum of DySb, clearly observed sharp peak of Sb 4*d* and Dy 4*f*, 5*s* and 5*p*, which indicates the good quality of the samples. (d),(e) Bulk-band calculations along multiple high symmetry points of DySb without and with the consideration of spin orbit coupling, respectively.

are marked on the bulk BZ with the Γ point established as the center and the X point as the corner of the surface BZ as indicated. Relative to the chemical potential, photoemission spectroscopy also provides the core level of the orbitals. Figure 2(c) shows the core levels in the 0-70eV binding energy range of DySb. We observe sharp peaks of Sb 4*d* (∼31 eV and ∼33 eV) and Dy 5*s* (∼ 47 eV), 5*p* (∼ 24 eV), and 4*f* (∼4 eV). The observation of sharp peaks suggests that the samples used in our spectroscopic measurements are of high quality.

The calculated bulk band structures of DySb presented here include one where spin orbit coupling (SOC) is not considered presented in Figure 2(d). The calculated band structure with SOC is shown in Figure 2(e) and it is clear that the distinct features of the bands are preserved from the non-SOC case. We see three hole-like bands at the Γ point and one electron-like band at the X point in both cases. Although, a gap-closing phenomena between the Dy *d* and Sb *p* states appears around the X point upon the inclusion of SOC. Upon careful inspection of the bands along the Γ and X point we observe band gaps of about 100 meV and 20 meV, respectively.

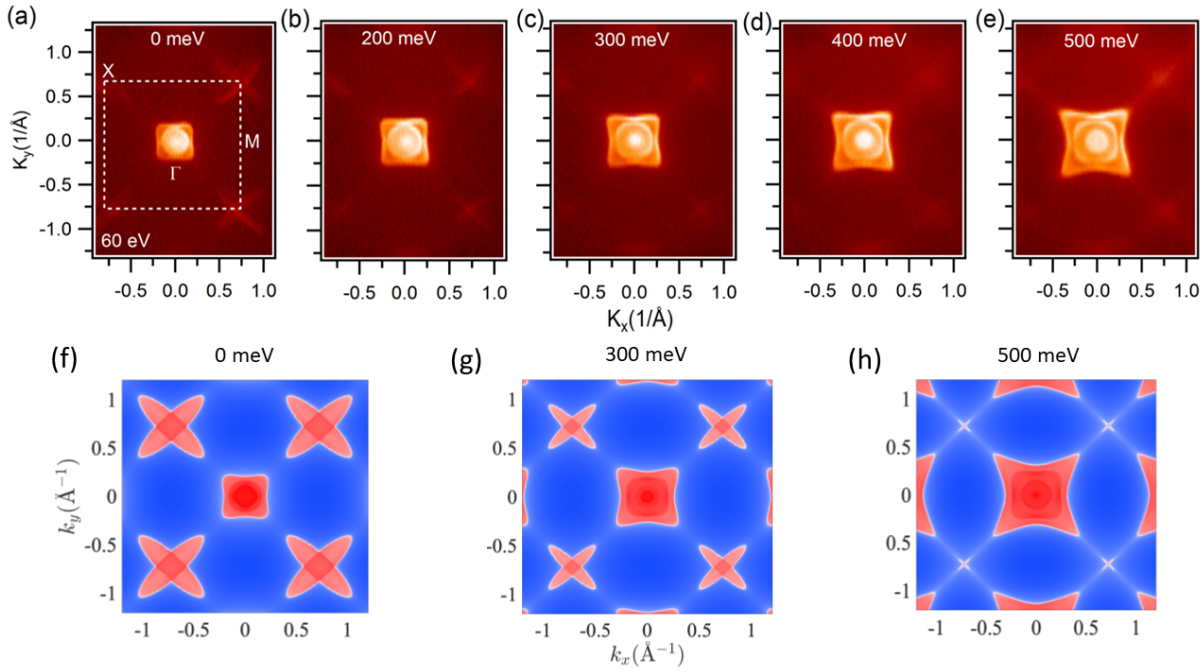

Figure 4.2: **Measured Fermi surface and constant energy contours of DySb.** (a-e) ARPES measured Fermi surface mapping and constant energy contours with an incident photon energy of 60 eV and a temperature of around 16 K. The binding energies are noted in the plots. (f-g) constant energy contour calculations using SCAN. The binding energies are noted in the plots. All the experiments were performed at SIS-HRPES end-station at SLS, PSI at a temperature around 16 K.

In order to ultimately determine the detailed electronic structure of DySb, we present the results of our systematic electronic structure study in our figures. Figure 2 displays the plot of the Fermi surface map and constant energy contours with various binding energies as marked in the plots, which are measured using a photon energy of 60 eV. Figure 2 (a) is the experimentally measured Fermi surface on the (001) surface and has the high symmetry points labeled on the plot where the center of the BZ is defined as the Γ point, X as the corner, and M as the middle point between the two corners. Figure 2(b)-(e) shows the constant energy contour plots with the binding energies noted in the plots. From the Figure 2 plots we observe a square-like outer Fermi pocket and a round inner pocket. A third band becomes more apparent within the circular pocket as higher

binding energy measurements are taken. Additionally, when moving to higher binding energies, the bands are observed to increase in size confirming that the bands around the center of the BZ have a hole like nature. It is also interesting to observe that the corners of the bands, especially the outer one, appear to stretch outwards towards the X points as we move towards higher binding energies. Setting our focus on the high symmetry X points at the Fermi level, two elliptically shaped pockets are easily observed. However, these elliptical pockets appear to initially shrink Figures 2(a-c) which would indicate that the bands are electron-like, but after a certain binding energy they fade and stretch towards the Γ points as the binding energy is increased Figures 2(d-e). This is expected as our calculations suggest a bulk gap at the X point between these ranges. From these observations, specifically that we observe a shrinking of the pockets from 0meV to 300meV and enlarging pockets from 400meV to 500meV, we can speculate that we have a bulk band gap somewhere between the 300meV to 400meV range. Figure 2(f-h) shows the calculated Fermi surface and constant contour plots. The calculated Fermi surface agrees with our experimental results. Our careful analysis confirms the bulk band gap at around 450 meV below the Fermi surface.

Experimental dispersion maps of various high symmetry directions and calculations are provided in Figure 3. Figure 3(a) is the experimentally measured band dispersion along the X-Γ-X direction at a photon energy of 60 eV and provides evidence of two hole bands crossing the Fermi level while the maxima of a third hole band reaches about 250 meV below the Fermi level. Additionally from this figure we observe a Dirac like structure at the Γ point with a potential crossing point at around 0.5 eV below the Fermi surface. The calculation presented in Figure 3(b) is of the dispersion map along the X-Γ-X direction. The calculation perfectly reconstructs the two hole bands crossing the Fermi level as well as the nature of the other bands, note that the calculated band structure covers a larger momentum range than the experimentally measured band structure. Figure 3(c) shows the measured dispersion map for the M-Γ-M direction and has a dispersion that is very similar to the

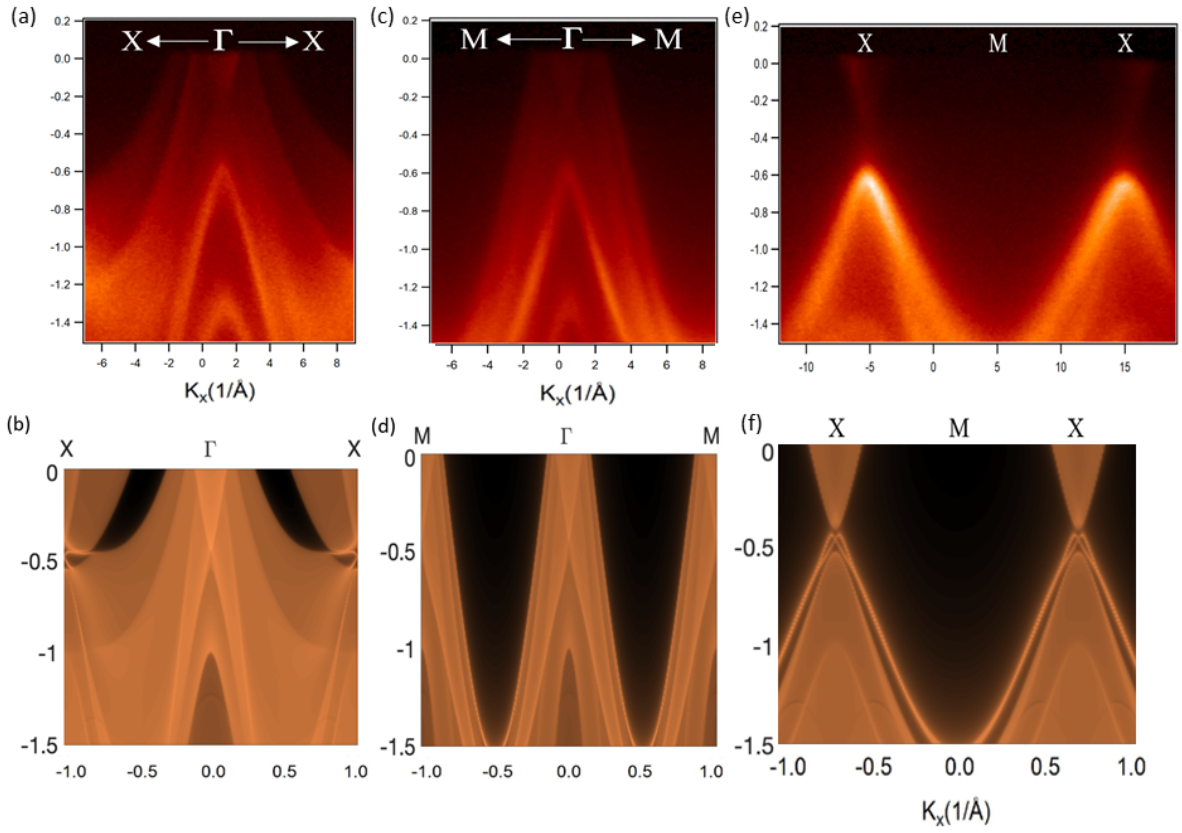

Figure 4.3: **Observation of Dirac like state in DySb.** (a) ARPES measured dispersion along the X-Γ-X direction with an incident photon energy of 70 eV at a temperature of 6 K. (b) SCAN calculations for the X-Γ-X direction. (c) ARPES measured dispersion along the M-Γ-M direction with an incident photon energy of 70 eV at a temperature of 30 K. (d) SCAN calculations for the M-Γ-M direction. (e) ARPES measured dispersion along the X-M-X direction with an incident photon energy of 60 eV at a temperature of 30 K. (f) SCAN calculations for the X-M-X direction. All these measurements were performed at SIS-HRPES end-station at SLS, PSI all calculations were done considering the "f" electrons as core electrons.

X-Γ-X direction shown in Figure 3(a) where two of the three hole bands are observed to cross the Fermi level. The calculation presented in Figure 3(d) is of the full M-Γ-M direction. Once again a major difference is that along the M-Γ-M direction, the bands appear to be much steeper and linear than those seen in the X-Γ-X direction. Figure 3(e) is the experimentally measured band structure along the X-M-X direction with a photon energy of 60 eV. This measured data provides

an interesting perspective of the high symmetry X point as at first glance it appears to have a sort of linear dispersion. Upon closer inspection a gap between the conduction and valence band can be observed. This observation indicates that it is not possible for DySb to be a topological Dirac semimetal. Additionally, parity calculations confirm that no band inversion exists in the X-Γ direction. Figure 3(f) is the SCAN calculations pertaining to the X-M-X direction and they heavily agree with the experimental observations in regards to the observed band dispersion and establish that a band gap of 20 meV exists at the X point. The Z_2 invariant is well defined as a continuous band gap between the valence and conduction bands exists. Using the evolution of Wannier charge centers [95], it is determined that the topological invariant $Z_2 = 0$, confirming that DySb is a trivial semimetal.

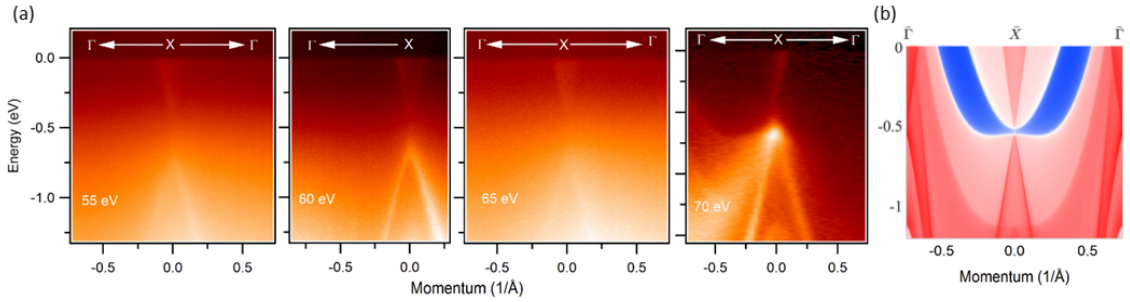

Figure 4.4: **Photon energy dependent measurements of the Γ-X-Γ direction in DySb.** The High symmetry X point is measured at various photon energies from 55 eV to 70 eV in increments of 5 eV steps where a Dirac-like linearly dispersive state is observed in each plot. It is important to note that the rightmost image with 70eV photon energy was taken at ALS beamline 10.0.1 with a different sample at 17 K, the rest of the measurements were performed at SIS-HRPES end-station at SLS, PSI at a temperature around 16 K.

Conclusion

Our systematic photoemission and theoretical analysis of DySb single crystals has provided us with sufficient enough information to make particular claims. To begin, our experimental ARPES

measurements indicate that a Dirac-like cone structure is present in the X point in the BZ of the DySb system, but the existence of a tiny band gap around 450 meV below the Fermi surface negates the possibility of a TSS existing in DySb. Both experimental and theoretical examination suggest that there is a 20 meV band gap at the high symmetry X point. Furthermore, DySb experiences an AFM transition at low temperatures and this provides a solid opportunity to study XMR and magnetism in a single material. Ultimately, our study realizes the presence of trivial states in DySb and conclude that it could potentially be a nearly perfect topological electron-hole compensated semimetal which would be a likely explanation for the origin of the large XMR seen in its paramagnetic phase.

α-$PdBi_2$

Majorana fermions hosted in topological superconductor materials (TSC) have been a fascinating topic of research for many years now. These unique materials hold promise of revolutionizing computing as we know it by providing a means to realize robust quantum computing. Superconducting members of the Pd-Bi binarys family have fallen in the spotlight as they serve as possible hosts for a topological superconducting phase due to their high spin-orbit coupling. As such, here we perform systematic angle-resolved photoemission spectroscopy (ARPES) measurements on fascinating material α-$PdBi_2$. The results from this study on this superconducting material with a $T_c = 1.7K$ has revealed a Dirac-state at 1.26 eV below the Fermi level at the Γ-point. α-$PdBi_2$ is also shown to be metallic as a result of the many band crossings observed from the ARPES measurements. By comparing our experimental measurements with theoretical predictions it is possible to reveal unique states in this system, by doing this we realize surface Rashba states extremely close to the Fermi level. The results from this investigation provide a means to develop a deeper understanding between topology and superconductivity in addition to the development of

new possible directions in the realm of quantum computing.

Introduction

It is well known that the class of quantum materials known as Topological Insulators (TIs) are a revolutionary milestone for the condensed matter sciences community. They are known for having an insulating bulk but hosting gapless spin-polarized surface states [1, 2]. These TIs are not only ideal materials for studying a multitude of unique physical phenomena, but they also have a strong potential for application in technologies that span from quantum computing to spintronics and other low-power technologies [1, 2, 51, 7, 8]. In regards to its potential applications in quantum computing, there have been many predictions that the elusive Majorana fermions could be realized at an interface between a superconductor and topological insulator [15, 16, 17, 18, 19, 20]. The interest in discovering a means to create robust qubits pushes research in this direction, as these Majorana fermion quasiparticles provide a promising means to develop such technologies. Materials that can realize Majorana particles have the ability to develop robust qubits, a property that allow these sensitive qubits to resist decoherence, which is common in non-topological qubits and results in a loss of function of the qubit. Many candidates that have the potential to host the long-sought-out Majorana fermions have been investigated due to this enormous potential for applications [21, 22, 23, 24]. Although there are not many instances of topological superconductivity (TSC) realized in real materials, there have been many instances of bulk topological superconductivity being realized in multiple materials. This includes half-Heusler materials [25, 26], superconductor-topological insulator and hybrid superconductor-semiconductor heterostructures [23, 27], point contact regions in Cd_3As_2 [29], highly pressured Sb_2Te_3 and Bi_2Te_3 [14, 31], And especially Sr- or Cu- intercalated Bi_2Se_3 [32, 33, 34, 35, 36, 37, 38].

There has been high interest in the Pd-Bi class of materials as they have been predicted as likely

hosts of topological superconductivity phenomena as a direct result of their high spin-orbit coupling (SOC). The investigations on the superconducting noncentrosymmetric α-PdBi have shown that a Dirac like dispersion exists around 700 meV below the fermi surface, not close enough to the chemical potential and thus denying the possibility of a topological superconducting surface state to exist within this material [71, 40, 41, 42]. Although a TSC insulating phase is possible to exist within this material, and due to its noncentrosymmetric nature and high SOC it is reasonable to expect a mixture of triplet and singlet pairing [40, 43]. The material β-$PdBi_2$ from the same family could also be predicted to host TSC states but upon closer examination it was found that its Dirac cone was 2.41 eV below the Fermi level [44] and measurements using point-contact Andreev reflection spectroscopy has shown that a TSC state does not exist within this system [45]. Moving on to the material α-$PdBi_2$, one with the same chemical composition as β-$PdBi_2$ but different arrangement, has been suggested to host interesting surface states within its system shown by penetration depth measurements as well as DFT [46, 47]. As such, a systematic study on the band structure of α-$PdBi_2$ had yet to be conducted until Dimitri et al. [48].

Here, we reveal our systematic study of the band structure of compound α-$PdBi_2$ using ARPES. A single crystal of α-$PdBi_2$ is examined above its Neel temperature, so it is studied outside of its superconducting state in this paper. A Dirac state is revealed at a binding energy of 1.26 eV below the Fermi surface. Additionally, states that are percieved to exhibit Rashba-type splitting are observed right next to the chemical potential. These experimental results are accurately reflected by the first-principles calculations. The overall observations on this compound are that a TSC surface state does not exist in α-$PdBi_2$ in its unmodified state, although potential tuning of the Fermi surface may allow for the existence of Dirac surface states.

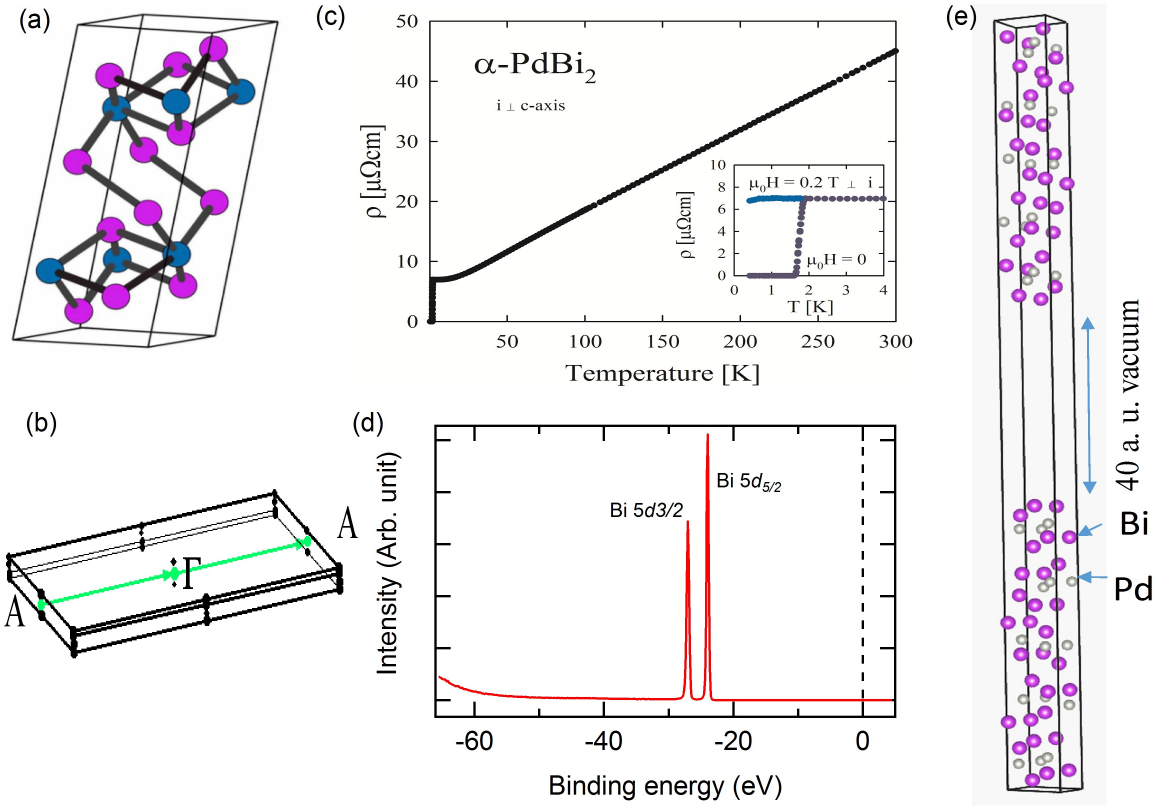

Figure 4.5: **α-PdBi$_2$ molecular structure and transport data** (a) Molecular structure of α-PdBi$_2$ where purple spheres are Bi atoms and blue spheres are Pd atoms (b) Momentum path in the 5 $\times$ 1 $\times$ 1 supercell used for DFT calculations of α-PdBi$_2$. (c) Temperature dependent resistivity measurements. (d) Core level spectrum (e) 5 $\times$ 1 $\times$ 1 supercell used for theoretical DFT calculations.

Results

The growth technique used to develop the α-PdBi$_2$ single crystals are described elsewhere [46]. Using X-ray spectroscopy and diffraction the crystals chemical composition and structure were determined to be α-PdBi$_2$. Beamline 10.0.1 at the Advance Light Source (ALS), Berkley was used to examine the single crystals of α-PdBi$_2$. The R4000 electron analyzer used had an energy resoulution of 20 meV and an angular resolution less than 0.2°. All measurements were performed between 10 - 80 K in a vacuum under 10^{-10}. The sample was also cleaved in situ with the cleav-

age plane being the (100) plane. To most accurately characterize the electronic band structure of α-$PdBi_2$, the experimental data obtained from ARPES was directly compared with the density functional theory (DFT) calculated band structure, which was directly projected onto a 2D Brillouin zone (BZ). The calculation techniques included using a FLAPW method inside the WIEN2k package [93].

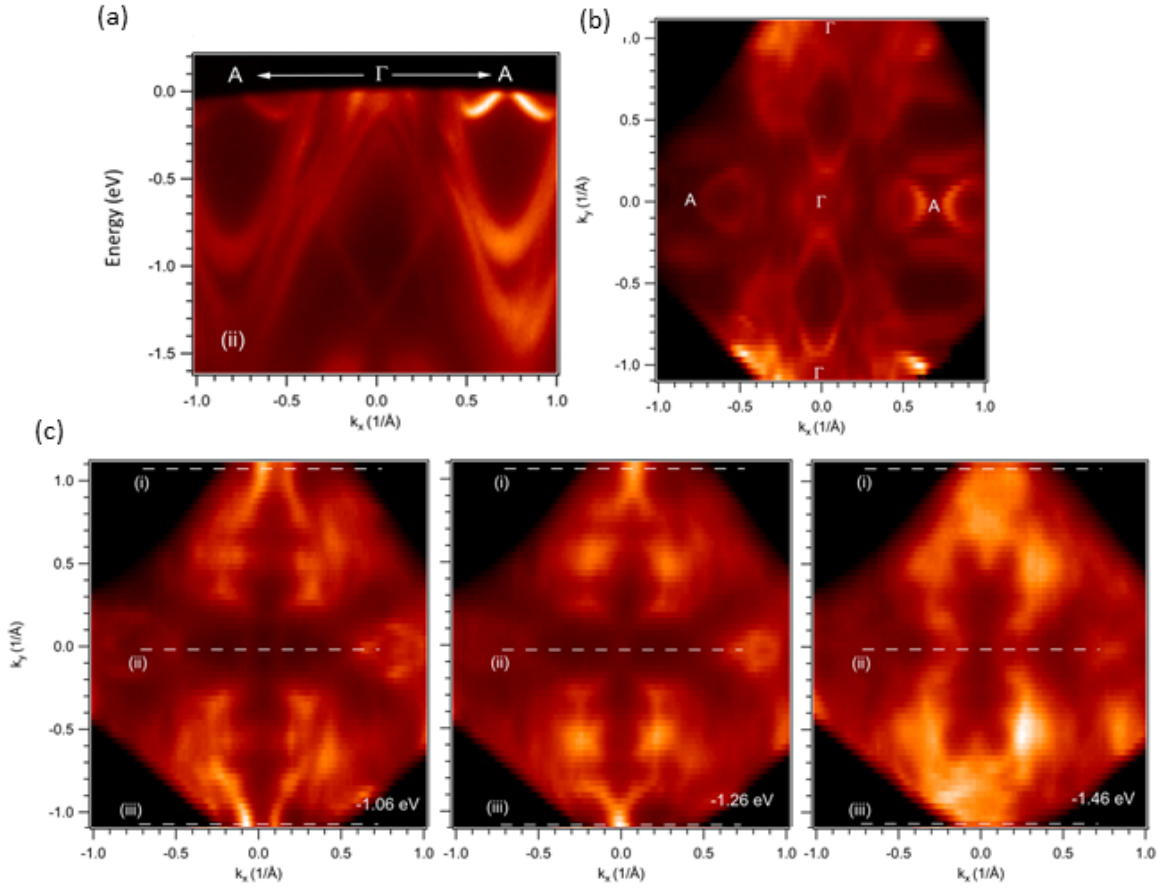

Figure 4.6: **Experimentally measured band structure of α-$PdBi_2$** (a) Electronic structure measurements cut along the A-Γ-A direction. (b) Fermi surface map of α-$PdBi_2$ (c) Binding energy measurments above, at and below the Dirac point

Analyzing the transport properties of α-$PdBi_2$ provides us with information that indicates a monoclinic centosymmetric unit cell with a space group of $C2/m$ and lattice parameters of a = 12.74

Å, b = 4.25 Å, c = 5.665 Å, $\alpha = \gamma = 90°$, and $\beta = 102.58°$ [49].In figure 1a we see the unit cell of α-$PdBi_2$ where the a-axis is its unique direction. For figure 1b we see the Brillouin Zone (BZ) divided by the A-Γ-A direction which is defined as the (100) surface. It is possible to see the high quality of the crystals used by graphing the electrical resistivity vs the electrical current flowing through the (100) plane, since the measurements match the expected values, the crystals are of high quality. From the graph it is observed that the compound has good metallic conductivity and at a T_c = 1.7 K it has a sharp transition into a superconducting state (Figure 1c) as was determined in other experiments [46]. Figure 1d is the α-$PdBi_2$ integrated ARPES spectrum measured over a large momentum window. As expected we see both the $5d_{3/2}$ and $5d_{5/2}$ orbital peaks at energies of E_B = 27 and 24 eV, respectively.

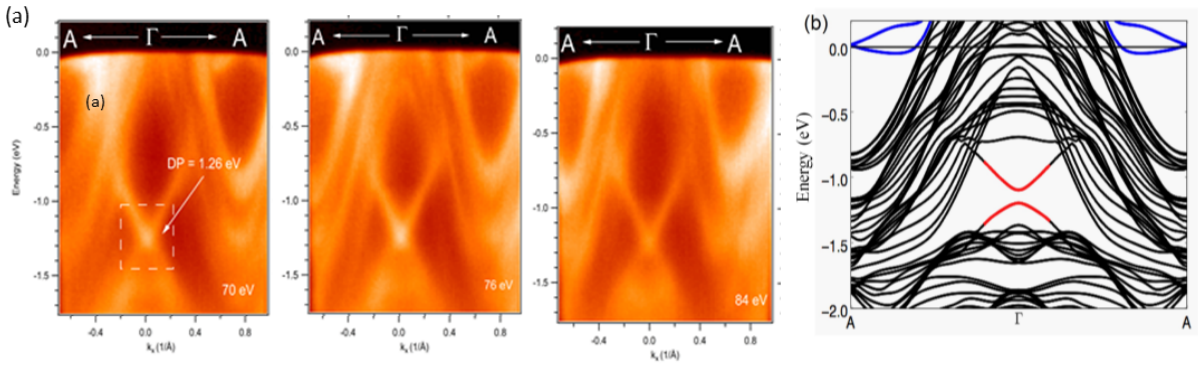

Figure 4.7: **Theory and Experimental comparison** (a) Dispersion map of α-$PdBi_2$ obtained at photon energies of 70, 76, and 84 eV

In figure 4.6(a) multiple valence bands are crossing the Fermi level indicating the metallic nature of this material, although by looking closely in the vicinity of the Fermi level in the top right section of the figure it is possible to observe some clear Rashba splitting. Additionally, a Dirac like state with linear dispersion can be observed at the Γ-point at around 1.26 eV below the Fermi level. A Fermi surface map measured with a photon energy of 50 eV can be seen in Figure 4.6(b), several oval shaped metallic pockets can be seen in the figure around the Γ (center) and A (edges) of the

Brillouin Zone. The constant energy contour plots can be seen in Figure 4.6(c) where the binding energies of 1.06, 1.26, and 1.46 eV below the Fermi level are shown to depict the band structure above, at, and below the Dirac point, respectively. Looking closer at the 1.26 eV measurement and it is possible to see a point like feature at the very center of the graph, corresponding to the Dirac point. It is difficult to obtain a clear resolution of the Dirac point though as a direct result of the multiple bulk bands present around the point, as that partially obscures the feature. As the measurements are moved to higher and lower binding energies from the 1.26 eV point, it is possible to see that the constant energy contours expand as would be expected when doing so from a Dirac point.

The next step is to determine the origin of the linearly dispersive bands tied to the Dirac point, in order to do so, the same cut along the A-Γ-A direction was made for 3 different photon energies as shown in Figure 4.7(a). The photon energies are 70, 76, and 84 eV, and in each the Dirac point is visible and does not alter or disperse between each of the measurements. This indicates that the Dirac state is surface originated and partially provides promising evidence for the existence of a topological surface state. Similarly, the Rashba-split states near the Fermi level also do not disperse with the photon energy, unlike the bulk bands that disperse and change as the photon energy is increased or decreased. This provides great evidence for surface originated states. Following this an analysis of the theory is important and as such Figure 4.7(b) provides the first-principles calculation of a $5 \times 1 \times 1$ supercell of α-$PdBi_2$ as is shown in Figure 4.5(e). As can be observed in Figure 4.7(b), we observe the Rashba-split states next to the Fermi level as well as the Dirac-like dispersion at the Γ-point. These calculations are in excellent agreement with the experimental measurements, although an apparent band gap can be seen in the calculations, this is attributed to the size effect as a result of the size of the slab calculations.

Finally, Figure 4.8 depicts the calculated band structure of the system, without (Figure 4.8(a)) and with (Figure 4.8(b-c)) spin-orbit coupling. There is a clear difference between the two sets of

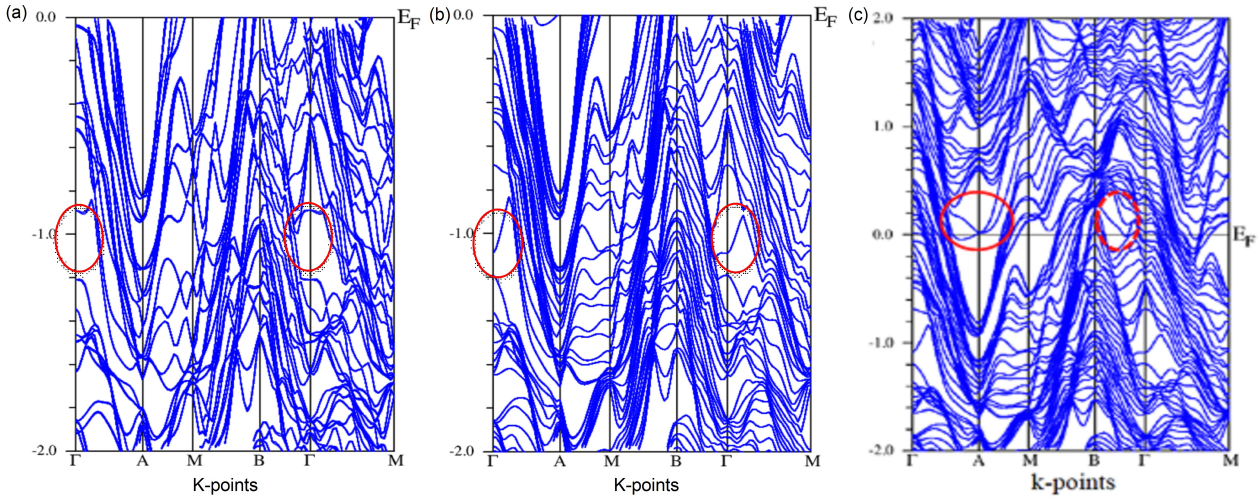

Figure 4.8: **Calculated band structures of α-PdBi$_2$** (a) Without SOC (b) With SOC (c) With SOC and a larger binding energy range extending over the Fermi level.

figures and observing around the Fermi level it is possible to see that when SOC is considered one can clearly see the Rashba-splitted states as are circled in Figure 4.8(c). It can also be seen that the around 1.26 eV the linearly dispersive bands of the Dirac-like state are greatly affected by the surface potential and spin-orbit coupling. The oval shapes in both Figure 4.8(a) and 4.8(b) show that once spin-orbit coupling is considered, the linearly dispersive states that characterize the Dirac-like state emerge. It is essential that a surface state is in play in order for this change to occur [47]. It is predicted that considering a larger slab geometry for calculations would result in a closed gap.

There are very identical features between the theory and experimental results at the Γ-point where the Dirac-like state forms around 1.26 eV below the Fermi level. Since an identical band structure is identified at a high symmetry point it is possible to claim that the Dirac state in this system originates from the surface but is directly tied to the surface potential. The calculations from the supercell further corroborate the surface originated nature of the Dirac-like dispersion. It is also

clear that the features around high symmetry point A are seen in both theory and experiment. This Rashba state next to the Fermi level is a momentum-dependent splitting that is driven by the degenerate surface state because of the troughs developed by spin-orbit coupling in the vicinity of the high symmetry A-point.

Conclusion

After both systematic experimental and theoretical analysis of the electronic structure of α-$PdBi_2$, a mostly surface originated Dirac state has been identified. It is found at 1.26 eV below the Fermi level. Since α-$PdBi_2$ also has a superconducting state, a topological superconducting state may be possible with some proper tuning of the Dirac state. There is also great interest in the Rashba-split states found next to the Fermi level which are likely governed by the surface potential. The Rashba-split states are in close proximity to a high symmetry point and the Fermi level, thus slight tuning would very likely result in the realization of spin-split Rashba states within α-$PdBi_2$. There is the possibility of realizing Majorana fermions at the interface between a superconductor and materials that exhibit Rashba-type spin-orbit coupling [13]. This study of α-$PdBi_2$ indicates that it is an exceptional material that has great potential to push new directions in condensed matter physics and may be a platform to realize topological phases in a superconducting material.

Preliminary Results on KFe_2Te_2

The centrosymmetric iron-based material KFe_2Te_2 provides a potential platform to study the interplay between magnetism and superconductivity within a nodal-line material. As seen in Figure 1(a), KFe_2Te_2 has a tetragonal $ThCr_2Si_2$ type unit cell with space group $I4/mmm$ (139) [11]. The bicollinear anti-ferromagnetic order of the Fe spins in the ground states have a magnetic mo-

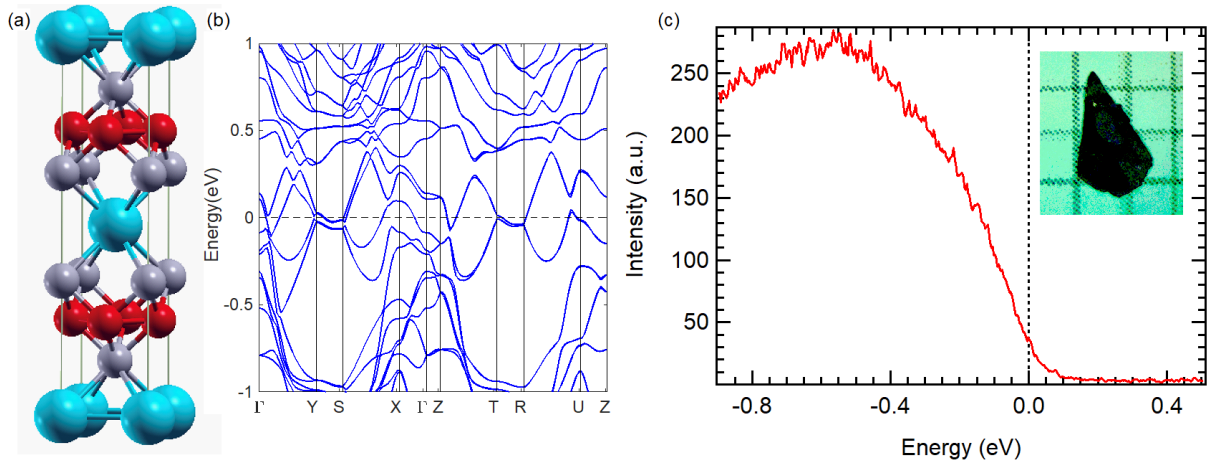

Figure 4.9: **Preliminary results for KFe_2Te_2.** (a) Molecular structure of KFe_2Te_2. (b) Band structure calculation for the Bicollinear anti-ferromagnetic order of KFe_2Te_2 with a magnetic moment of 2.6 μ_B (c) The integrated energy distribution curve for KFe_2Te_2. Inset shows a sample of KFe_2Te_2 where the sample is approximately 5 mm at its longest and 3 mm at its widest.

ment calculated to be around $2.6\mu_B$ [54]. As transport data as well as other experimental data on KFe_2Te_2 has been lacking, but with experimental data on selenium doped $KFe_1.5S_2$ (T_C = 26.3 K) [97] and undoped $K_0.8Fe_2Se_2$ ($T_C \sim 31$ K) [10], it was calculated that the density of states (DOS) at the Fermi level grows as the chalcogenide element of KFe_2Ch_2 (*Ch* = Chalcogenide) moves from S $\rightarrow$ Se $\rightarrow$ Te. This in addition to the Fe-*Ch* bond angles becoming closer to the ideal tetrahedron angles as it transitions to the heavier chalcogenide are favorable for the formation of superconducting states [11].

KFe_2Te_2 shows great promise to potentially host multi-modal phenomena within its system. For one it has a huge magnetic moment, additionally, Figure 1(b) shows a very interesting set of measurements especially between the Y-S and T-R high symmetry direction as well as between Γ-X. With more investigation we will have a better idea of what this could indicate in the bigger picture of realizing multi-modal materials.

Unfortunately, I had major plans to perform a systematic experimental study of this material using

ARPES at the ALS facility at Berkeley, but the assigned beamtime was canceled due to COVID-19 reasons. As such I was not able to complete the experimental analysis of this material. The theoretical analysis of this material shows great promise though. A quick analysis of the Y-S and T-R high symmetry directions show a band structure that could potentially host either a Weyl or Nodal-line state. Especially since this sample is magnetic this would have been an extremely interesting material to analyze. Without the experimental analysis of this material no specific claims can be made and thus this will be left for future works.

CHAPTER 5: CONCLUSION

The major results to come from the three materials investigated in this thesis are solid but still require further investigation in order to develop a deeper understanding of both the individual materials and their families. DySb was shown to be topologically trivial in its normal state, but it establishes an extremely solid foundation to better understand f-electron systems, rare earth monopnictides, as well as Dirac-like systems. Perhaps it still has a few surprises once it is investigated under its Neel temperature. As for α-$PdBi_2$, it comes off as an extremely promising material to push the realm of realizing qubits with Rashba split states and Majorana fermions. Additionally it does host a Dirac like state and it has much to be investigated at lower temperatures. Finally, no concrete evidence was determined with KFe_2Te_2 as a result of unforeseeable circumstances, yet with only the theoretical information on the system it still shows that it has the potential to be an incredible magnetic material that hosts multiple phenomena.

Future Work

There is still much to do regarding the investigation of the material brought forth in this thesis. DySb still needs to be investigated at temperatures below its Neel temperature. It would be nice to be able to perform spin-resolved ARPES on α-$PdBi_2$ to determine the nature of the Rashba-states, additionally if interesting results come from the spin-resolved ARPES then attempting to building devices with α-$PdBi_2$ would be the next step. And finally KFe_2Te_2 still requires a whole heap of experimental measurments to be performed on it including traditional ARPES. All I know is that I still have a lot to do and explore when it comes to even just these materials.

Closing Remarks

The major idea that this thesis intended to address is to explore the fermion quasiparticles. Fermions fall into one of three categories, Dirac, Majorana, and Weyl. As such the intentions of this thesis was to explore and investigate three different materials that had the potential to host each of these fermionic quasiparticle states. DySb explored Dirac fermions, α-$PdBi_2$ explored Majorana fermions, and finally it was predicted that KFe_2Te_2 could host Weyl fermions. Ultimately this led to a process that has taught me the first principles of the physics behind materials and the especially the ins and outs of the scientific method. From this thesis I will have an immensely strong foundation to continue research in the condensed matter field and continually push the frontier and direction of materials science.

LIST OF REFERENCES

[1] M. Z. Hasan, and C. L. Kane, Rev. Mod. Phys. **82**, 3045-3067 (2010).

[2] X.-L. Qi, and S.-C. Zhang, Rev. Mod. Phys. **83**, 1057 (2011).

[3] M. Z. Hasan, S.-Y. Xu, and M. Neupane, John Wiley & Sons, Chapter 4, 55-96 (2015).

[4] P. R. Wallace, Phys. Rev. 71, 622 (1947)

[5] A. Bansil et al., Colloquium: Topological band theory, Rev. Mod. Phys. 88, 021004 (2016)

[6] S. Borisenko, et al. Time-reversal symmetry breaking type-II Weyl state inYbMnBi2. arXiv:1507.04847 (2015)

[7] Y. Kamihara *et al.*, J. Am. Chem. Soc. **130**(11), 3296 (2008).

[8] M. Rotter *et al.*, Phys. Rev. B **78**(2), 020503 (2008).

[9] F. C. Hsu *et al.*, Proc. Natl. Acad. Sci. USA **105**(38), 14262 (2008).

[10] J. Guo *et al.*, Phys. Rev. B **82**, 180520(R) (2010).

[11] I. R. Shein and A. L. Ivanovskii, J. Supercond. Nov. Magn. **24**, 2215 (2011).

[12] M. Z. Hasan, and C. L. Kane, *Rev. Mod. Phys.* **82**, 3045-3067 (2010).

[13] Andrew C. Potter and Patrick A. Lee Phys. Rev. B 85, 094516 (2012)

[14] X.-L. Qi, and S.-C. Zhang, *Rev. Mod. Phys.* **83**, 1057 (2011).

[15] L. Fu, and C. L. Kane, Phys. Rev. Lett. 100, 096407 (2008).

[16] X.-l. Qi, T. L. Hughes, S. Raghu, and S.-C. Zhang, Phys. Rev. Lett. 102, 187001 (2009).

[17] M. Sato, and S. Fujimoto, Phys. Rev. B 79, 094504 (2009).

[18] A. Vorontsov, I. Vekhter, and M. Eschrig, Phys. Rev. Lett. 101, 127003 (2008).

[19] Y. Tanaka, Y. Mizuno, T. Yokoyama, K. Yada, and M. Sato, Phys. Rev. Lett. 105, 097002 (2010).

[20] M. Sato, and S. Fujimoto, Phys. Rev. Lett. 105, 217001 (2010).

[21] A. Y. Kitaev, Phys. Usp. 44, 131 (2001).

[22] Q. L. He, L. Pan, A. L. Stern, E. C. Burks, X. Che, G.Yin, J.g Wang, B. Lian, Q. Zhou, E. S. Choi, K. Mu- rata, X. Kou, Z. Chen, T. Nie, Q. Shao, Y. Fan, S.-C. Zhang, K. Liu, J. Xia, and K. L. Wang, Science 357, 294 (2017).

[23] V. Mourik, K. Zuo, S. M. Frolov, S. R. Plissard, E. P. A. M. Bakkers, and L. P. Kouwenhoven, Science 336, 1003 (2012).

[24] S. Nadj-Perge, I. K. Drozdov, J. Li, H. Chen, S. Jeon, J. Seo, A. H. MacDonald, B. A. Bernevig, and A. Yazdani, Science 346, 602 (2014).

[25] S. Chadov, X. Qi, J. Kbler, G. H. Fecher, C. Felser and S. C. Zhang, Nat. Mater. 9, 541-545 (2010).

[26] H. Lin, L. A. Wray, Y. Xia, S. Xu, S. Jia, R. J. Cava, A. Bansil, and M. Z. Hasan, Nat. Mater. 9, 546-549 (2010).

[27] S.-Y. Xu, N. Alidoust, I. Belopolski, A. Richardella, C. Liu, M. Neupane, G. Bian, S.-H. Huang, R. Sankar, C. Fang, B. Dellabetta, W. Dai, Qi Li, M. J. Gilbert, F. Chou, N. Samarth, and M. Z. Hasan, Nat. Phys. 10, 943 (2014).

[28] Y. Xia, D. Qian, D. Hsieh, L. Wray, A. Pal, H. Lin, A. Bansil, D. Grauer, Y. S. Hor, R. J. Cava, and M. Z. Hasan, *Nat. Phys.* **5**, 398 (2009).

[29] H. Wang, H. Wang, H. Liu, H. Lu, W. Yang, S. Jia, X.-J. Liu, X. C. Xie, J. Wei, and J. Wang, Nat. Mat. 15, 38 (2016).

[30] J. L. Zhang, S. J. Zhang, H. M. Weng, W. Zhang, L. X. Yang, Q. Q. Liu, S. M. Feng, X. C. Wang, R. C. Yu, L. Z. Cao, L. Wang, W. G. Yang, H. Z. Liu, W. Y. Zhao, S. C. Zhang, X. Dai, Z. Fanga, and C. Q. Jin, Proc. Natl. Acad. Sci. 108, 24 (2011).

[31] J. Zhu, J. L. Zhang, P. P. Kong, S. J. Zhang, X. H. Yu,J. L. Zhu, Q. Q. Liu, X. Li, R. C. Yu, R. Ahuja, W. G. Yang, G. Y. Shen, H. K. Mao, H. M. Weng, X. Dai, Z. Fang, Y. C. Zhao, and C. Q. Jin, Sci. Rep. 3, 2016 (2013).

[32] Y. S. Hor, A. J. Williams, J. G. Checkelsky, P. Roushan, J. Seo, Q. Xu, H. W. Zandbergen, A. Yazdani, N. P. Ong, and R. J. Cava, Phys. Rev. Lett. 104, 05701 (2010).

[33] L. A. Wray, S.-Y. Xu, Y. Xia, Y. S. Hor, D. Qian, A. V. Fedorov, H. Lin, A. Bansil, R. J. Cava, and M. Z. Hasan, Nat. Phys. 6, 855 (2010).

[34] M. Kriener, K. Segawa, Z. Ren, S. Sasaki, and Y. Ando, Phys. Rev. Lett. 106, 127004 (2011).

[35] S. Sasaki, M. Kriener, K. Segawa, K. Yada, Y. Tanaka, M. Sato, and Y. Ando, Phys. Rev. Lett. 107, 217001 (2011).

[36] Z. Liu, X. Yao, J. Shao, M. Zuo, L. Pi, S. Tan, C. Zhang, and Y. Zhang, J. Am. Chem. Soc. 137, 10512 (2015).

[37] Shruti, V. K. Maurya, P. Neha, P. Srivastava, and S. Patnaik, arXiv:1505.05394v1 (2015).

[38] M. Neupane, Y. Ishida, R. Sankar, J.-X. Zhu, D. S. Sanchez, I. Belopolski, S.-Y. Xu, N. Alidoust, M. M. Hosen, S. Shin, F. Chou, M. Z. Hasan, and Tomasz Durakiewicz, Sci. Rep. 6, 22557 (2016).

[39] Z. Sun, M. Enayat, A. Maldonado, C. Lithgow, E. Yelland, D. C. Peets, A. Yaresko, A. P. Schnyder, and P. Wahl, Nat. Commun. 6, 6633 (2015).

[40] M. Neupane, N. Alidoust, M. M. Hosen, J.-X. Zhu, K. Dimitri, S.-Y. Xu, N. Dhakal, R. Sankar, I. Belopolski, D. S. Sanchez, T.-R. Chang, H.-T. Jeng, K. Miyamoto, T. Okuda, H. Lin, A. Bansil, D. Kaczorowski, F. C. Chou, M. Z. Hasan and T. Durakiewicz, Nat. Commun. 7, 13315 (2016).

[41] S. Thirupathaiah, S. Ghosh, R. Jha, E. D. L. Rienks, K. Dolui, V. V. Ravi Kishore, B. Buchner, T. Das, V. P. S. Awana, D. D. Sarma, and J. Fink, Phys. Rev. Lett. 117, 177001 (2016).

[42] H.M. Benia, E. Rampi, C. Trainer, C.M. Yim, A. Maldonado, D.C. Peets, A. Stoehr, U. Starke, K. Kern, A. Yaresko, G. Levy, A. Damascelli, C.R. Ast, A.P. Schnyder, P. Wahl, Phys. Rev. B 94, 121407 (2016).

[43] B. Joshi, A. Thamizhavel, and S. Ramakrishnan, Phys. Rev. B 84, 064518 (2011).

[44] M. Sakano, K. Okawa, M. Kanou, H. Sanjo, T. Okuda, T. Sasagawa, and K. Ishizaka, Nat Commun. 6, 8595 (2015)

[45] L. Che, T. Le, C. Q. Xu, X. Z. Xing, Z. Shi, X. Xu, and X. Lu, Phys. Rev. B 94, 024519 (2016).

[46] S. Mitra, K. Okawa, S. K. Sudheesh, T. Sasagawa, J.-X. Zhu, and E. Chia, Phys. Rev. B 95, 134519 (2017).

[47] H. Choi, M. Neupane, T. Sasagawa, E. E. M. Chia, and J.-X. Zhu, arXiv: 1704.03445v1 (2017).

[48] K. Dimitri, M. M. Hosen, G. Dhakal, H. Choi, F. Kabir, D. Kaczorowski, T. Durakiewicz, J.-X. Zhu, and M. Neupane, Phys. Rev. B 97, 144514 (2018).

[49] N. N. Zhuravlev, Zh. Eksp. Teor. Fiz. 32, 1305 (1957).

[50]

[51] M. Z. Hasan, S.-Y. Xu, and M. Neupane, (John Wiley and Sons, New York, 2015).

[52] Z. Wang, H. Weng, Q. Wu, Xi Dai, and Z. Fang, *Phys. Rev. B* **88**, 125427 (2013).

[53] M. Neupane, S.-Y. Xu, R. Sankar, N. Alidoust, G. Bian, C. Liu, I. Belopolski, T.-R. Chang, H.-T. Jeng, H. Lin, A. Bansil, F.-C. Chou, and M. Z. Hasan, *Nat. Commun.* **5**, 3786 (2014).

[54] S. Y. Xu, *et al.* 2015 *Science* **349**, 613

[55] B. Q. Lv, *et al.* 2015 *Phys. Rev. X* **5**, 031013

[56] M. Neupane, I. Belopolski, M. M. Hosen, D. S. Sanchez, R. Sankar, M. Szlawska, S.-Y. Xu, K. Dimitri, N. Dhakal, P. Maldonado, P. M. Oppeneer, D. Kaczorowski, F. C. Chou, M. Z. Hasan, and T. Durakiewicz, *Phys. Rev. B* **93**, 201104 (2016).

[57] R. Yoshomi, A. Tsukazaki, K. Kikutake, J. G. Checkelsky, K. S. Takahashi, M. Kawasaki and Y. Tokura, *Nat. Mater.* **23**, 253-257 (2014).

[58] M. Zeng, C. Fang, G. Chang, Y.-A. Chen, T. Hsieh, A. Bansil, H. Lin and Liang Fu, arXiv:1504.03492 (2015).

[59] J. He, C. Zhang, N. J. Ghimire, T. Liang, C. Jia, J. Jiang, S. Tang, S. Chen, Y. He, S.-K. Mo, C.C. Hwang, M. Hashimoto, D.H. Lu, B. Moritz, T.P. Devereaux, Y.L. Chen, J.F. Mitchell and Z.-X. Shen, *Phys. Rev. Lett.* **117**, 267201 (2016).

[60] H.-Y. Yang, T. Nummy, H. Li, S. Jaszewski, M. Abramchuk, D. S. Dessau and F. Tafti, *Phys. Rev. B* **96**, 235128 (2017).

[61] O. Pavlosiuk, P. Swatek, Da. Kaczorowski and P. Winiewski, Magnetoresistance in LuBi and YBi semimetals due to nearly perfect carrier compensation, arXiv:1712.08433v2 (2018).

[62] C. Guo, C. Cao, M. Smidman, F. Wu, Y. Zhang, F. Steglich, F.-C. Zhang, and H. Yuan, *Quantum Mater.* **2**, 39 (2017).

[63] D. D. Liang, Y. J. Wang, C. Y. Xi, W. L. Zhen, J. Yang, L. Pi, W. K. Zhu , and C. J. Zhang *APL Mater.* **6**, 086105 (2018)

[64] Q.-H. Yu, Y.-Y. Wang, R. Lou, P.-J. Guo, s. Xu, K. Liu, S. Wang and T.-L. Xia, *EPL* **119**, 17002 (2017).

[65] H. -Y. Yang, J. Gaudet, A. A. Aczel, D. E. Graf, P. Blaha, B. D. Gaulin and F. Tafti, arXiv:1805.12260 (2018).

[66] Neupane M. *et al.* 2013 *Nat. Commun.* **4**, 2991

[67] Neupane M. *et al.* 2015 *Phys. Rev. Lett.* **114**, 016403

[68] Neupane M *et al.* 2015 *Phys. Rev. Lett.* **115**, 116801

[69] Tafti F. F., Gibson Q. D., Kushwaha S. K., Haldolaarachchige N., and Cava R. J. 2016 *Nat. Phys.* **12**, 272–7

[70] Tafti F. F., Gibson Q. D., Kushwaha S. K., Krizan J. W., Haldolaarachchige N. and Cava R. J. 2016 *Proc. Natl. Acad. Sci. USA* **113**, E3475

[71] S. Sun, Q. Wang, P.-J. Guo, K. Liu, and H. Lei, *New J. Phys.* **18**, 082002 (2016)

[72] Guo P. J., Yang H. C., Liu K., and Lu Z. Y. 2016 *Phys. Rev. B* **93**, 235142

[73] Kumar N., Shekhar C., Wu S. C., Leermakers I., Zeitler U., Yan B., and Felser C. 2016 *Phys. Rev. B* **93**, 241106(R)

[74] L. K. Zeng, R. Lou, D. S. Wu, Q. N. Xu, P. J. Guo, L. Y. Kong, Y. G. Zhong, J. Z. Ma, B. B. Fu, P. Richard, P. Wang, G. T. Liu, L. Lu, Y. B. Huang, C. Fang, S. S. Sun, Q.Wang, L.Wang, Y. G. Shi, H. M.Weng, H. C. Lei, K. Liu, S. C.Wang, T. Qian, J. L. Luo, and H. Ding, *Phys. Rev. Lett.* **117**, 127204 (2016).

[75] H. Oinuma, S. Souma, D. Takane, T. Nakamura, K. Nakayama, T. Mitsuhashi, K. Horiba, H. Kumigashira, M. Yoshida, A. Ochiai, T. Takahashi, and T. Sato, *Phys. Rev. B* **96**, 041120 (2017).

[76] O. Pavlosiuk, M. Kleinert, P. Swatek, D. Kaczorowski, and P. Wisniewski, *Sci. Rep.* **7**, 12822 (2017).

[77] K. Kuroda, M. Ochi, H. S. Suzuki, M. Hirayama, M. Nakayama, R. Noguchi, C. Bareille, S. Akebi, S. Kunisada, T. Muro, M. D.Watson, H. Kitazawa, Y. Haga, T. K. Kim, M. Hoesch, S. Shin, R. Arita, and T. Kondo, *Phys. Rev. Lett.* **120**, 086402 (2018).

[78] J. J. Song, F. Tang,W. Zhou, Y. Fang, H. L. Yu, Z. D. Han, B. Qian, X. F. Jiang, D. H.Wang, and Y.W. Du, *J. Mater. Chem. C* **6**, 3026 (2018).

[79] Y.Wang, J. H. Yu, Y. Q.Wang, C. Y. Xi, L. S. Ling, S. L. Zhang, J. R.Wang, Y. M. Xiong, T. Han, H. Han, J. Yang, J. Gong, L. Luo, W. Tong, L. Zhang, Z. Qu, Y. Y. Han, W. K. Zhu, L. Pi, X. G. Wan, C. Zhang, and Y. Zhang, *Phys. Rev. B* **97**, 115133 (2018).

[80] Y.-Y. Wang, H. Zhang, X.-Q. Lu, L.-L. Sun, S. Xu, Z.-Y. Lu, K. Liu, S. Zhou, and T.-L. Xia, *Phys. Rev. B* **97**, 085137 (2018).

[81] G. Busch and O, Vogt, *J. Appl. Phys.* **39**, 1334 (1968).

[82] E. Bucher, R. J. Birgeneau, J. P. Maita, G. P. Felcher, and T. O. Brun, *Phys. Rev. Lett.* **28**, 746 (1972).

[83] F. L´evy, *Phys. Kondens. Mater.* **10**, 85 (1969).

[84] Canfield P. C. and Fisk Z., 1992 *Phil. Mag. B* **65**, 1117

[85] Blöchl, P. E. Projector augmented-wave method. *Phys. Rev. B* **50**, 17953 (1994).

[86] Kresse, G. and Hafner, j, *Phys. Rev. B* **47**, 558 (1993).

[87] Kresse, G. and Furthmuller, *J. Computational Materials Science* **6**, 15 (1996).

[88] Sun, J., Ruzsinszky, A. and Perdew, J. P. , *Phys. Rev. Lett.* **115**, 036402 (2015).

[89] Mostofi, A. A., et al., *Comput. Phys. Commun.* **185**, 2309 (2014).

[90] Q. Wu, S. Zhang, H.-F. Song, M. Troyer, and A. A. Soluyanov, *Comput. Phys. Commun.* **224**, 405 (2018).

[91] Lopez Sancho, M. P., Lopez Sancho J. M. and Rubio, J., *J. Phys. F: Met. Phys.* **14**, 1205 (1984).

[92] Lopez Sancho, M. P., Lopez Sancho J. M. and Rubio, J., *J. Phys. F: Met. Phys.* **15**, 851 (1985).

[93] Blaha J, Schwarz P, Madsen K, Kvasnicka G K H and Luitz D 2001

[94] Abdusalyamova M, Shokirov H, Rakhmatov O 1990 *J. Less Common Met.* **166**, 221

[95] Yu, R., Qi, X. L., Bernevig, A., Fang, Z. and Dai, X. , *Phys. Rev. B* **84**, 075119 (2011).

[96] X.-G. Xu and W. Li, Front. Phys. **10**(4), 107403 (2015).

[97] J. G. Guo *et al.*, Phys. Rev. B **85**, 054507 (2012)

[98] M. Neupane *et al.*, Nat. Commun. **5**, 3786 (2014).

[99] M. Neupane *et al.*, J. Phys.: Condens. Mat. **28**, 23LT02 (2016).

[100] Keung, Wai-Yee; Senjanović, Goran (1983). Physical Review Letters. 50 (19): 1427–1430.

[101] A. A. Burkov, M. D. Hook, and L. Balents, Topological nodal semimetals. Phys. Rev. B 84, 235126 (2011)

[102] R. Yoshomi et al., Nat. Mater. 13, 253-257 (2014).

[103] O. Pavlosiuk, P. Swatek and P. Wisniewski, Sci. Rep. 6, 38691 (2016).

[104] X. Huang et al., Phys. Rev. X 5, 031023 (2015).

[105] T. Liang et al., Nat. Mater. 14, 280 (2015).

[106] J. Nayak et al., Nat.Commun. 8, 13942 (2017).

[107] R. Lou et al., Phys. Rev. B 95, 115140 (2017).

[108] T. J. Nummy et al., npj Quantum Mater. 3, 24 (2018).

[109] B. Feng et al., Phys. Rev. B 97, 155153 (2018)